THE JOURNAL OF PHYSICAL CHEMISTRY A

Article

Cite This: J. Phys. Chem. A 2019, 123, 5517−5524

pubs.acs.org/JPCA

Face-Sharing Homo- and Hetero-Bitetrahexahedral Superatomic Molecules $M_1M_2@Li_{20}$ (M_1/M_2 = Ti and W)

Lijuan Yan*

College of Electronics & Information Engineering, Guangdong Ocean University, Zhanjiang 524088, China

Supporting Information

ABSTRACT: Superatoms, being a class of clusters with chemical behavior similar to atoms, can be used as building blocks for constructing novel functional materials. Here, superatomic molecules $M_1M_2@Li_{20}$ (M_1/M_2 = Ti and W) are built with our recently discovered tetrahexahedral superatoms $Ti@Li_{14}$ and $W@Li_{14}$. A low-energy face-sharing bi-tetrahexahedral structure with a high symmetry of D_{6h} is identified by global minimum structure search and frequency calculations. The number of shared Li atoms amounts to 6, which is rarely seen before. Molecular orbital and chemical bonding analyses reveal that although isolated superatoms $Ti@Li_{14}$ and $W@Li_{14}$ are nonmagnetic, $Ti_2@Li_{20}$ is an open-shell superatomic molecule with a magnetic moment of 2 μ_B, whereas for $W_2@Li_{20}$, the electronic shell remains closed. In both $Ti_2@Li_{20}$ and $W_2@Li_{20}$, a quadruple superbonding between superatoms is found. Interestingly, an assembly of two hetero-tetrahexahedral superatoms $Ti@Li_{14}$ and $W@Li_{14}$ also gives a face-sharing bi-tetrahexahedral structure but with a notable dipole moment. This study provides a basic understanding for the superatomic bonding of $Ti@Li_{14}$ and $W@Li_{14}$, which may aid their application in developing multi-superatom molecules or even bulk crystals.

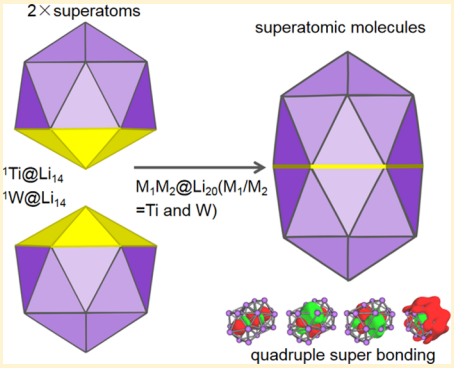

1. INTRODUCTION

By tuning size, geometry, composition, and charge state, the properties of atomic clusters can be easily tailored, offering abundant building blocks for cluster-assembled materials with targeted functions.[1−3] As a special type of atomic clusters, superatoms are proposed to mimic the chemical behavior of simple elements in the periodic table. The valence electrons in superatoms fill in a series of atom-like orbitals, with the orbital shapes resemble to those of atoms.[4] However, different from atoms, the electronic filling order of superatoms generally does not follow the Hund's rule because of the effects of atomic deformations. For metal clusters, their electronic sequences can be understood by the jellium model,[5,6] where the valence electrons are subject to a uniform positive potential derived from the atomic nuclei and inner electrons. The resulting electronic levels of metal clusters are $|1S^2|1P^6|1D^{10}|2S^21F^{14}|$, and so forth, where 2, 8, 18, 20, 34, and 40, and so forth, electrons correspond to magic clusters or inert element superatoms. The superatom concept has been applied successfully to explain the stability of many metal clusters, such as the large peaks at the size of 8, 20, and 40 in mass spectra of sodium clusters,[7] the resistant of Al_n^- (n = 13, 23, 37, etc.) toward oxygen etching,[8] and the superhalogen character of Al_{13}.[4]

The high stability of superatoms makes them promising for designing cluster-assembled materials. However, the structures of pure superatoms are often distorted to low symmetry upon cluster assembly. A potential route to solve this problem is by ligand protection, such as thiolates (RS)[9] and phosphines (PR_3).[10] A typical ligand-protected superatom is the icosahedral Au_{13}^{5+} (8e),[11−13] which possesses high stability and has been isolated in the experiment. Via different bonding modes, many dimeric structures of Au_{13}^{5+} are constructed, for example, a vertex-sharing Au_{25}^{9+} (16e) core found in the $[Au_{25}(SR)_5(PPh_3)_{10}Cl_2]^{2+}$ cluster,[14,15] a face-sharing Au_{23}^{9+} (14e) core formed in the $Au_{38}(SR)_{24}$ cluster,[16,17] and the nonsharing Au_{26}^{10+} (16e) core identified in $Au_{40}(SR)_{24}$.[18,19] With properly ligand protected, the superatom-assembled materials are accessible.

In a superatom context, binary superatoms, composed of two different elements, are another intriguing field, such as the endohedral $M@Si_n$[20−25] and $X@Al_{12}$ clusters,[26−31] where properties can be precisely controlled by changing the doped elements M/X while keeping the whole geometric structure. For the Ti-doped silicon $Ti@Si_{16}$ cluster,[20,21,24] there are 68 valence electrons with a filling order of $1S^21P^61D^{10}1F^{14}2S^21G^{18}2P^62D^{10}$, analogous to the noble gas atoms. When the central atom Ti is replaced by its neighboring element Sc or Ta, the corresponding properties of $Sc@Si_{16}$ cluster[20] and $Ta@Si_{16}$ cluster[22,24,25] change to be halogen-like or alkali-metal-like, respectively. Similarly, the Cu- or Si-doped Al_{12} cluster can be tuned to mimic a phosphorus or noble gas atom, respectively.[27,29] Above all, on the basis of the same geometric structures, the properties of binary superatoms can

Received: February 26, 2019
Revised: May 7, 2019
Published: May 29, 2019

DOI: 10.1021/acs.jpca.9b01855
J. Phys. Chem. A 2019, 123, 5517−5524

be easily tailored by the variation of endohedral atoms. Moreover, compared with pure superatoms, the characteristics of binary superatoms are often augmented, being more suited to real-life applications.[32] However, there are still few studies on the assembled materials from binary superatoms.

Noteworthy, using Li clusters as a test case, Cheng and Yang proposed the super valence bond (SVB) model in 2013, in which superatoms could form delocalized superbonding by sharing both valence pairs and nuclei with other superatoms or atoms.[33] On the basis of the SVB model, the electronic stability of some prolate metal clusters and some ligand-protected clusters has been successfully understood,[34−37] where the shell closure of superatoms is obtained by superatoms−superatoms or superatoms-atom bonding. Moreover, taking double-icosahedral motif of 26e $Li_{20}Mg_3$ and 30e $Li_{18}Mg_3Al_2$ as examples,[38] Cheng et al. reveal the existence of quintuple superbonding (σ, 2π, 2δ) between two icosahedral superatoms, further expanding the community of chemical bonds. As a way of assembling materials from binary superatoms, the SVB model gives a referable direction.

Recently, we have found a series of new binary superatoms, namely, TM@Li_{14} (TM = Sc, Ti, V, Y, Zr, Nb, Hf, Ta, and W),[39] which present a D_{6d} symmetry tetrahexahedral structure with the cage composed of 14 lithium atoms and the center occupied by a transition-metal atom. Among them, Ti@Li_{14} and W@Li_{14}, of which all of the effective valence electrons are paired, are chosen as building blocks and a new type of stable face-sharing bitetrahexahedral superatomic molecules M_1M_2@Li_{20} (M_1/M_2 = Ti and W) are constructed in this paper. The structural, electronic, and magnetic properties of M_1M_2@Li_{20} (M_1/M_2 = Ti and W) are systematically studied, which reveal three important findings: first, when the two superatoms bond, up to six atoms are shared, whereas in common clusters, the shared number of atoms is usually 0−3. Second, despite the nonmagnetic feature of the two superatoms, the superatomic molecules could be magnetic. Last, a quadruple superbonding between the two superatoms is discovered.

2. COMPUTATIONAL DETAILS

The low-energy structures of M_1M_2@Li_{20} (M_1/M_2 = Ti and W) clusters are located by Crystal structure AnaLYsis by Particle Swarm Optimization (CALYSPO),[40] which is an efficient structure prediction method. Then, the obtained low-energy isomers are fully optimized at the density functional theory level implemented in the Gaussian16 package.[41] All of these low-energy isomers are confirmed as true local minima by frequency calculations. To choose valid gradient-corrected exchange−correlation functionals for transition-metal compounds,[42,43] three functionals including pure functional PW91,[44] meta-GGA functional M06-L,[45] and hybrid functional TPSSh[46] are adopted with SDD as the basis set.[47] In addition, different spin multiplicities (SMs) are considered for each isomer, where the SM of ground state is identified with the lowest energy. All of the pictures presented in the paper are based on the PW91/SDD calculations, and molecular visualization is performed using Multiwfn_3.6.[48]

3. RESULTS AND DISCUSSION

3.1. Geometric Structure. The geometric structures of the face-sharing bitetrahexahedral clusters Ti_2@Li_{20} and W_2@Li_{20} have a D_{6h} symmetry, whereas their corresponding building superatoms Ti@Li_{14} and W@Li_{14} possess the D_{6d} symmetry.[39] As shown in Figure 1, the formation of superatomic molecules can be viewed as the fusion of two Ti@Li_{14} or W@Li_{14}

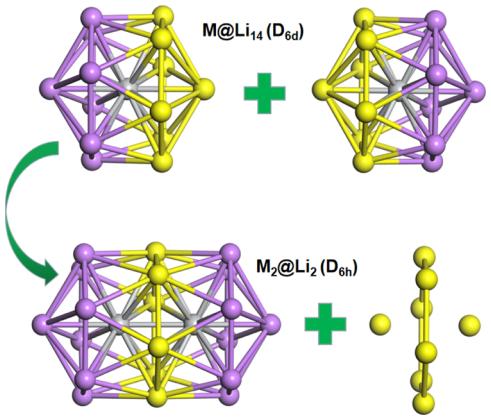

Figure 1. Diagrams of the formation of M_1M_2@Li_{20} (M_1, M_2 = Ti and W) from superatoms Ti@Li_{14} or W@Li_{14}.

superatoms along the C_6 axis, where the approaching top atom of one superatom is replaced by the endohedral transition-metal atom of another superatom, whereas eight redundant lithium atoms are removed with a six-membered Li ring shared between the two superatoms. Frequency calculations check that they are all true local minima. Through structure prediction by CALYSPO code, the face-sharing bitetrahexahedral Ti_2@Li_{20} is confirmed as the lowest energy isomer (A1 in Figure 2), where the nearest neighbor low-energy structure (A2) is 0.04 eV higher in energy at the calculations of PW91/SDD level. In fact, the A2 structure can

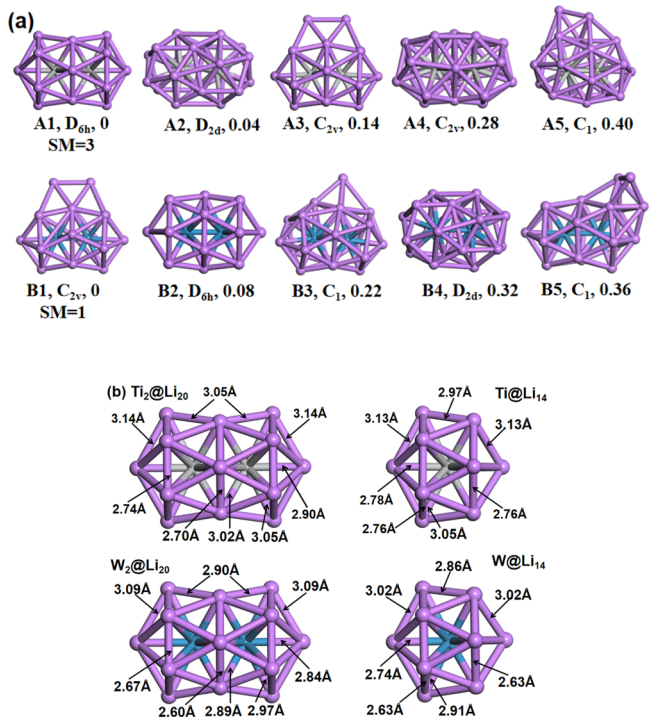

Figure 2. (a) Low-energy structures with the symmetry and the relative energies in eV for Ti_2@Li_{20} and W_2@Li_{20} at PW91/SDD levels, where the SMs of all of the isomers are 3 for Ti_2@Li_{20} and 1 for W_2@Li_{20}. (b) Bond lengths of the D_{6h} symmetry Ti_2@Li_{20}, W_2@Li_{20}, and their respective building units.

DOI: 10.1021/acs.jpca.9b01855
J. Phys. Chem. A 2019, 123, 5517−5524

Table 1. Results of the Calculated Symmetry, the Fragmentation Energy (E_f), the Binding Energy (E_b) per Atom, the Embedding Energy (D_e), HOMO−LUMO Gaps (E_{gap}), the Dipole Moments (d), and the Total Magnetic Moment (μ_s) of Ti_2@Li_{20} and W_2@Li_{20} with D_{6h} symmetry

M_1M_2	methods	symm.	E_f (eV)	E_b (eV)	D_e (eV)	E_{gap} (eV)	d (D)	μ_s (μ_B)
Ti_2	PW91	D_{6h}	1.25	1.58	11.6	0.35	0	2
	M06L		1.40	1.67	11.2	0.30		
	TPSSH		1.23	1.52	10.1	0.76		
TiW	PW91	C_{6v}	1.13	1.77	15.6	0.31	1.58	0
	M06L		1.31	1.81	14.3	0.40	2.15	
	TPSSH		1.00	1.67	13.6	0.76	1.71	
W_2	PW91	D_{6h}	1.16	1.95	19.7	0.48	0	0
	M06L		1.28	1.95	17.5	0.65		
	TPSSH		1.07	1.84	17.3	0.85		
Li_{22}[a]	PW91	C_1	1.27	1.17		0.38	0	1
	M06L		1.33	1.27		0.36		
	TPSSH		1.30	1.17		0.73		

[a]The lowest energy structures of Li_{22}, Li_{21}, and Li_{20} are obtained by CALYPSO code, Li_{20} refs.[40,56]

be viewed as an isosupermolecule of the face-sharing bitetrahexahedral Ti_2@Li_{20}, where isosupermolecules are proposed by Yang and co-workers[49] and defined as those clusters with difference structures but resembling each other in electronic structures. As for W_2@Li_{20} clusters, the face-sharing bitetrahexahedral structure is metastable and lies above the C_{2v} symmetry lowest-energy isomer by 0.08 eV. The corresponding isosupermolecule (B4) is also found.

Compared to the superatom monomer, the Li−Li bond lengths of the face-sharing bitetrahexahedral Ti_2@Li_{20} along the axis are elongated by 0.08 Å in the middle (2.97 Å for Ti@Li_{14} and 3.05 Å for Ti_2@Li_{20}), whereas they are almost unchanged at both ends (3.13 Å for Ti@Li_{14} and 3.14 Å for Ti_2@Li_{20}). Along the vertical direction of the axis, all of the Li−Li bond lengths are shortened by 0.06 and 0.02 Å at the sharing face and the ends (2.76 Å for Ti@Li_{14}, 2.70 and 2.74 Å for Ti_2@Li_{20}), respectively. Differently, for the face-sharing bitetrahexahedral W_2@Li_{20}, all of the Li−Li bond lengths along the axis are elongated by 0.04 and 0.07 Å at the middle and ends (2.86 and 3.02 Å for W@Li_{14}, and 2.90 and 3.09 Å for W_2@Li_{20}), respectively. Along the vertical axis direction, the Li−Li bond lengths are shortened by 0.03 Å near the sharing face (2.63 Å for W@Li_{14} and 2.60 Å for W_2@Li_{20}), whereas at both ends, they are elongated by 0.04 Å (2.63 Å for W@Li_{14} and 2.67 Å for W_2@Li_{20}). The changes of Li−Li bond lengths imply that W_2@Li_{20} is elongated larger along the axis than Ti_2@Li_{20}, which affects their stability.

3.2. Relative Stability. To investigate the stability of the face-sharing bitetrahexahedral clusters M_1M_2@Li_{20} (M_1/M_2 = Ti and W), their average binding energy (E_b) and fragmentation energy (E_f) are calculated, which are respectively defined by the following formulas

$$E_b(M_1M_2@Li_{20}) = \frac{E(M_1) + E(M_2) + 20E(Li) - E(M_1M_2@Li_{20})}{22}$$

$$E_f(M_1M_2@Li_{20}) = E(M_1M_2@Li_{19}) + E(Li) - E(M_1M_2@Li_{20})$$

In the above formulas, M_1 and M_2 denote the dopant Ti or W atom. $E(M_1M_2@Li_{20})$ represents the total energy of the face-sharing bitetrahexahedral clusters M_1M_2@Li_{20} (M_1/M_2 = Ti and W), and $E(M_1M_2@Li_{19})$ is the total energy of their corresponding fragments M_1M_2@Li_{19} by taking off one lithium atom from M_1M_2@Li_{20} (M_1/M_2 = Ti and W). E(Li) and $E(M_1/M_2)$ represent the total energy of the free-state Li atom and dopant atom, respectively.

In addition, the embedding energy indicating the feasibility of fusing transition-metal atoms into a cage is also calculated, which is defined as

$$D_e(M_1M_2@Li_{20}) = E(\text{shell}) + E(\text{core}) - E(M_1M_2@Li_{20})$$

where the total energies of the outer shell, center dopants, and complexes are denoted as E(shell), E(core), and $E(M_1M_2@Li_{20})$, respectively. Using such definition, a positive D_e value means that the encapsulation of dopants into the cage is favored thermodynamically.

The calculated results are summarized in Table 1. Compared to the pure Li_{22} cluster, the E_b of M_1M_2@Li_{20} (M_1/M_2 = Ti and W) is substantially increased, which indicates that doping with transition-metal atoms can significantly enhance their stability. The E_f of M_1M_2@Li_{20} (M_1/M_2 = Ti and W) is decreasing with the increasement of electron counts, so the clusters with more electrons dissociate easier. All of the values of D_e are positive, demonstrating the feasibility of doping the transition-metal atom into the Li_{20} cage.

The energy gaps (E_{gap}) between the highest occupied molecular orbital (HOMO) and lowest unoccupied molecular orbital (LUMO) are also calculated to examine their electronic stability. The E_{gap} values of Ti_2@Li_{20}, TiW@Li_{20}, and W_2@Li_{20} are 0.35, 0.31, and 0.48 eV, respectively, at the calculation level of PW91/SDD. Comparing to the gaps of typical magnetic superatoms, these gaps are moderate, for example, V@Na_8 (0.69 eV),[50] VNa_8^- (0.42 eV),[51] Pb@Mn_{12}@Pb_{20} (0.38 eV),[52] $MnSr_9$ (0.35 eV),[53] and so forth. Besides, the standard GGA functionals often underestimate the gaps, and thus the hybrid functional TPSSH is further applied to get more accurate gaps. At the calculation level of TPSSH/SDD, the E_{gap} values of Ti_2@Li_{20}, TiW@Li_{20}, and W_2@Li_{20} are found to be 0.76, 0.76, and 0.85 eV, respectively, as shown in Table 1.

3.3. Electronic Properties. On the basis of above discussions, the D_{6h} symmetry face-sharing bitetrahexahedral complexes Ti_2@Li_{20} and W_2@Li_{20} have high average binding energies, faired fragmentation energies, and moderate HOMO−LUMO gaps. All of these results suggest that Ti_2@Li_{20} and W_2@Li_{20} can be good candidates for the superatomic

DOI: 10.1021/acs.jpca.9b01855
J. Phys. Chem. A 2019, 123, 5517−5524

molecule, which is further confirmed by the analyses of MOs and chemical bonding patterns.

For $Ti_2@Li_{20}$, the number of total effective valence electrons is 28, where one ($2s^1$) and four ($3d^24s^2$) effective valence electrons are offered by a lithium atom and a titanium atom, respectively. According to the SVB model,[33] the face-sharing bi-tetrahexahedral $Ti_2@Li_{20}$ is assembled by two $Ti@Li_{14}^{4+}$ (14e) superatoms with an open electronic configuration.

$$Ti_2@Li_{20}(28e) = 2 \times Ti@Li_{14}^{4+}(14e) - 8Li^+$$

The equation means that eight Li^+ nuclei (six on the sharing face and two at the top) are removed for the reduction of the electron volume. However, $Ti@Li_{14}^{4+}$ (14e) is not stable. For simplicity, the building unit $Ti@Li_{14}$ superatom is adopted, of which the electronic configuration is $1S^21P^61D^{10}$ with all the effective valence electrons paired following the 18-electron rule. The analysis of the face-sharing bi-tetrahexahedral $W_2@Li_{20}$ is similar, where the electronic configuration of the building unit $W@Li_{14}$ is $1S^21P^61D^{10}2S^2$, fulfilling the 20-electron rule.

To discover the chemical bonding patterns of the face-sharing bitetrahexahedral complexes $Ti_2@Li_{20}$ and $W_2@Li_{20}$, their canonical Kohn−Sham MOs of the valence shell are first analyzed. The MO diagrams of $Ti_2@Li_{20}$ are given in Figure 3, and its schematic MO energy-level diagrams are plotted in Figure 4 for clarity. The first two sets MOs of $Ti_2@Li_{20}$ (σ_{1s} and σ^*_{1s}) are formed by two 1s superatomic orbitals (SAOs). The next two doubly degenerate sets MOs (π_{1p_x,p_y} and $\pi^*_{1p_x,p_y}$) and two sets (σ_{1p_z} and $\sigma^*_{1p_z}$) are composed of four $1p_x$ and $1p_y$ SAOs and two $1p_z$ SAOs, respectively. The MOs constructed from 1d SAOs are indicated by a number for clear. Then, the two doubly degenerate sets MOs ($\delta_{1d_{x^2-y^2,xy}}$ and $\delta^*_{1d_{x^2-y^2,xy}}$) and two doubly degenerate sets MOs [$\pi_{1d_{xz,yz}}$ and $\pi^*_{1d_{xz,yz}}$ (unlabeled)] consist of four $1d_{x^2-y^2,xy}$ SAOs and four $1d_{xz,yz}$ SAOs, respectively, where the antibonding orbitals $\delta^*_{1d_{x^2-y^2,xy}}$ of β and $\pi^*_{1d_{xz,yz}}$ of $\alpha\beta$ are unoccupied. The 38th occupied MO of α is $\sigma_{1d_{z^2}}$, mainly constructed from $1d_{z^2}$ electrons and a slight 2s electrons, which corresponds to the 47th unoccupied MO for β, and their antibonding MOs $\sigma^*_{1d_{z^2}}$ are not marked because of locating at a high-energy level. The two sets MOs (σ_{2s} and σ^*_{2s}) are composed of two 2s SAOs, where σ_{2s} is the 38th occupied MO for β, corresponding to the first unoccupied MO of α. Therefore, the electronic configuration of $Ti_2@Li_{20}$ is $(\sigma_{1s})^2(\sigma^*_{1s})^2(\pi_{1p_x,1p_y})^4(\pi^*_{1p_x,1p_y})^4(\sigma_{1p_z})^2(\delta_{1d_{x^2-y^2,xy}})^4(\sigma_{1d_{z^2}})_\alpha{}^1(\sigma_{2s})_\beta{}^1(\pi_{1d_{xz,yz}})^4(\sigma^*_{1p_z})^2(\delta^*_{1d_{x^2-y^2,xy}})_\alpha{}^2(\delta^*_{1d_{x^2-y^2,xy}})_\beta{}^0(\sigma_{2s})_\alpha{}^0(\sigma^*_{2s})_\beta{}^0(\sigma_{1dz^2})_\beta{}^0$, where the energy difference between $(\delta^*_{1d_{x^2-y^2,xy}})_\alpha$ and $(\delta^*_{1d_{x^2-y^2,xy}})_\beta$ forms its HOMO−LUMO gap (0.76 eV/TPSSh). The face-sharing bitetrahexahedral $Ti_2@Li_{20}$ is with a magnetic moment of 2 μ_B.

For complex $W_2@Li_{20}$, the number of total effective valence electrons is 32, where each tungsten atom offers six ($5d^46s^2$) effective valence electrons. From the canonical MOs of $W_2@Li_{20}$ given in Figure 3 and its schematic representation of Figure 4, the eight MOs, including two sets (σ_{1s} and σ^*_{1s}), two doubly degenerate sets (π_{1p_x,p_y} and $\pi^*_{1p_x,p_y}$), and two sets (σ_{1p_z} and $\sigma^*_{1p_z}$), are composed of two 1s SAOs, four $1p_{x,y}$ SAOs, and two $1p_z$ SAOs, respectively, which are corresponding to four super lone pair (LP) orbitals belonging to each superatom ($1S^21P^6$). The MOs marked with the numbers 31, 32, and 33 are bonding orbitals $\pi_{1d_{xz,yz}}$ and $\sigma_{1d_{z^2}}$, constructed from $1d_{xz,yz}$ and $1d_{z^2}$ SAOs, respectively, and their corresponding antibonding orbitals $\pi^*_{1d_{xz,yz}}$ and $\sigma^*_{1d_{z^2}}$ are 2.89 and 3.80 eV higher in energy, respectively. Thus, only the antibonding orbitals $\pi^*_{1d_{xz,yz}}$ (52 and 53) are shown in Figure 3. The two doubly degenerate sets MOs ($\delta_{1d_{x^2-y^2,xy}}$ and $\delta^*_{1d_{x^2-y^2,xy}}$) labeled with the number 36, 37, and 42, 43, respectively, are constituted by four $1d_{x^2-y^2,xy}$ SAOs. The next two sets MOs (σ_{2s} and σ^*_{2s}) are from two 2s SAOs, where the antibonding orbitals σ^*_{2s} are unoccupied. Hence, the electronic configuration of $W_2@Li_{20}$ is $(\sigma_{1s})^2(\sigma^*_{1s})^2(\pi_{1d_{xz,yz}})^4(\sigma_{1d_{z^2}})^2(\pi_{1p_x,1p_y})^4(\delta_{1d_{x^2-y^2,xy}})^4(\pi^*_{1p_x,1p_y})^4(\sigma_{1p_z})^2(\sigma^*_{1p_z})^2(\delta^*_{1d_{x^2-y^2,xy}})^4(\sigma_{2s})^2(\sigma^*_{2s})^0$. With all of the valence electrons paired, the face-sharing bitetrahexahedral $W_2@Li_{20}$ is nonmagnatic. The energy difference between σ_{2s} and σ^*_{2s} orbitals is its HOMO−LUMO gap (0.85 eV/TPSSh).

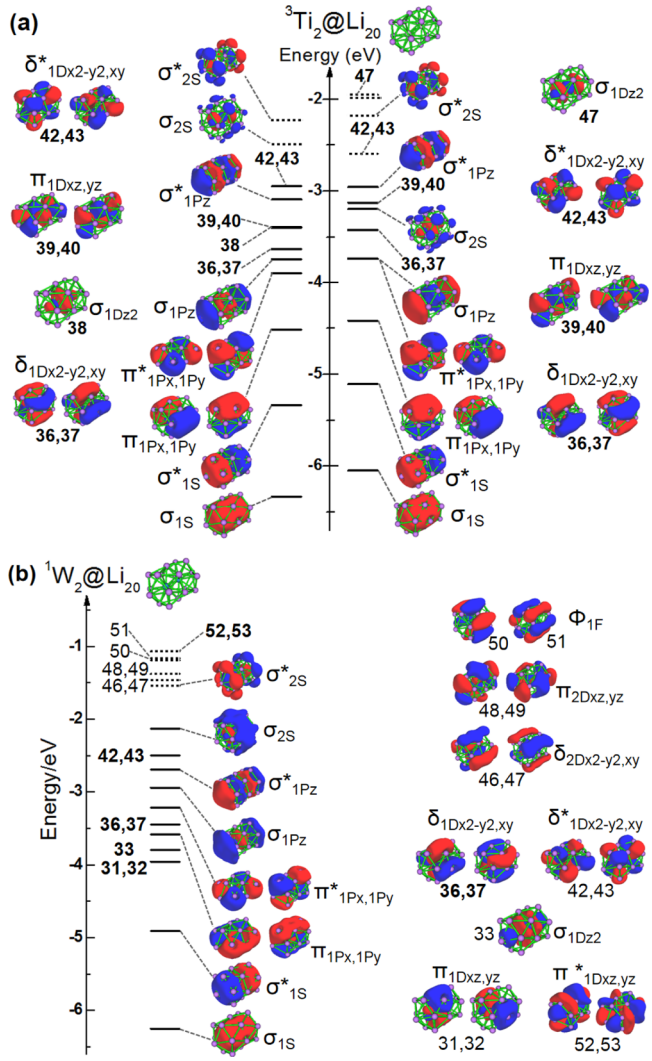

Figure 3. Kohn−Sham MOs diagrams of the face-sharing bi-tetrahexahedral superatomic molecules (a) $Ti_2@Li_{20}$ and (b) $W_2@Li_{20}$.

DOI: 10.1021/acs.jpca.9b01855
J. Phys. Chem. A 2019, 123, 5517−5524

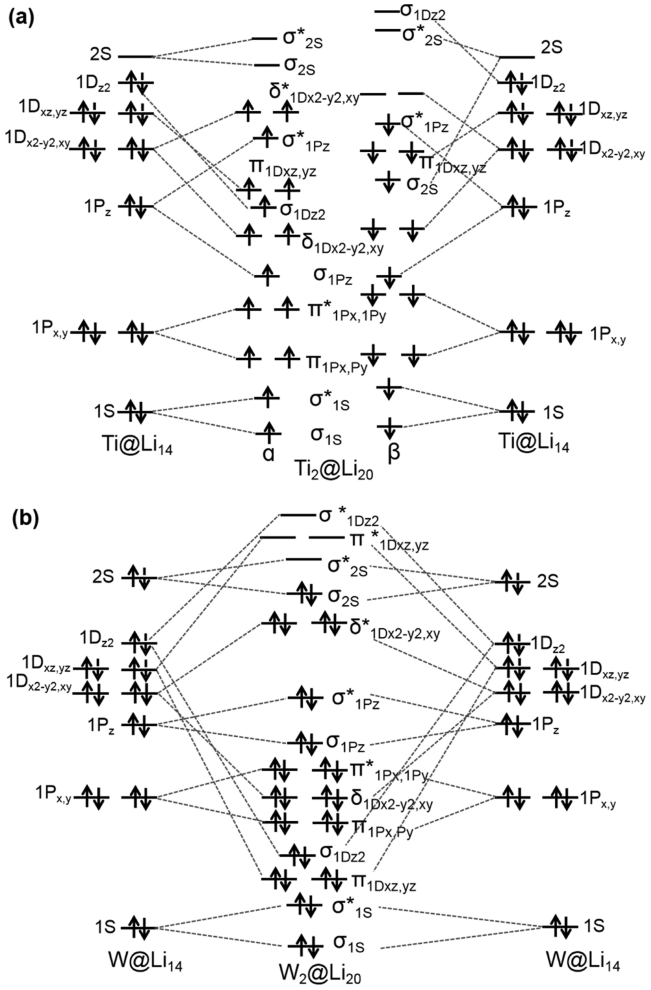

Figure 4. Schematic representation of the MO energy-level diagrams for the face-sharing bi-tetrahexahedral superatomic molecules (a) $Ti_2@Li_{20}$ and (b) $W_2@Li_{20}$.

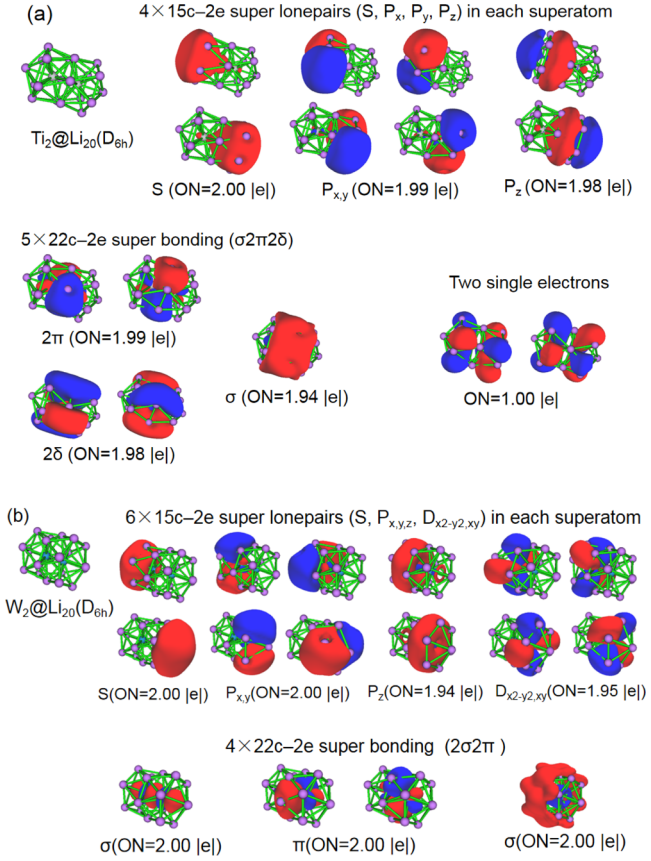

Figure 5. AdNDP localized natural bonding orbitals of the face-sharing bi-tetrahexahedral superatomic molecules (a) $Ti_2@Li_{20}$ and (b) $W_2@Li_{20}$.

From the canonical MOs, both $Ti_2@Li_{20}$ and $W_2@Li_{20}$ can be viewed as superatomic molecules.

To further confirm the existence of superatom−superatom superbonding in $Ti_2@Li_{20}$ and $W_2@Li_{20}$, a vivid view on their chemical bonding patterns is given by the adaptive natural density partitioning (AdNDP) method,[54] which is a chemical bonding analysis tool developed by Zubarev and Boldyrev. As shown in Figure 5, the $Ti_2@Li_{20}$ cluster has four 15-center 2-electron (15c−2e) super LPs (super s, p_x, p_y, and p_z) located in each superatom, and five 22c−2e superatom−superatom bonds (σ, 2π, 2δ) in the whole cluster. The remaining two electrons are two single electrons filled in the 42nd and 43rd MOs $\delta^*_{1d_{x^2-y^2,xy}}$ of α. Thus, the super bond order of $Ti_2@Li_{20}$ is four because of the occupied antibonding orbitals $\delta^*_{1d_{x^2-y^2,xy}}$ of α. For $W_2@Li_{20}$, the AdNDP analysis gives six 15c−2e super LPs (super s, p_x, p_y, p_z, $d_{x^2-y^2}$, and d_{xy}) in each superatom, four 22c−2e superatom−superatom bonds (2σ, 2π) in the whole cluster. Correspondingly, the super bond order of $W_2@Li_{20}$ is also four. The super LPs, super $\sigma 2\pi 2\delta$-bonds, and super $2\sigma 2\pi$-bonds for $Ti_2@Li_{20}$ and $W_2@Li_{20}$ are all with high occupancy numbers. Therefore, the face-sharing bitetrahexahedral complexes $Ti_2@Li_{20}$ and $W_2@Li_{20}$ can be viewed as superatomic molecules. Such a bonding pattern is similar to those of 26e $Li_{20}Mg_3$ and 30e $Li_{18}Mg_3Al_2$ clusters, which have a high bond order with quintuple superbonding ($\sigma 2\pi 2\delta$).[38] As comparison, the MO diagrams and bonding patterns of their corresponding isosupermolecules are given in Figures S1 and S2, which can be viewed as the assembly of two 14c superatoms $Ti@Li_{13}$ and $W@Li_{13}$ shared by six nuclei.

On the basis of the above analysis, the face-sharing bitetrahexahedral $Ti_2@Li_{20}$ and $W_2@Li_{20}$ clusters are identified as superatomic molecules in geometric and electronic shells. From SAOs to MOs, the orders of 1D energy level for $W_2@Li_{20}$ change a lot as the schematic representations of MO energy-level diagrams shown in Figure 4. The positions of $\pi_{1d_{xz,yz}}$ and $\sigma_{1d_{z^2}}$ MOs energy levels for $W_2@Li_{20}$ are lower than that of $Ti_2@Li_{20}$. The differences can be derived from their structures. Compared to $Ti_2@Li_{20}$, where the Li−Li bond lengths at both ends along the axis remain the lengths of its building unit $Ti@Li_{14}$, the corresponding Li−Li bond lengths of $W_2@Li_{20}$ are elongated by 0.07 Å. Meanwhile, the Li−W bond lengths of $W_2@Li_{20}$ in the inner away from the sharing face are elongated by 0.06 Å, whereas the corresponding Li−Ti bond lengths of $Ti_2@Li_{20}$ is almost unchanged. The more elongated geometric structure of $W_2@Li_{20}$ leads to lower positions of $\pi_{1d_{xz,yz}}$ and $\sigma_{1d_{z^2}}$ MOs, also suggesting that the interactions of its two superatoms are long range. Further, the stability of building units is needed to consider. For the tetrahexahedral superatoms, the 18-electron systems are easier to exist than the 20-electron systems, where all of the IVB transition-metal elements, namely, Ti, Zr, and Hf atoms embedded in the center of the Li_{14} cage, the formed

DOI: 10.1021/acs.jpca.9b01855
J. Phys. Chem. A 2019, 123, 5517−5524

superatoms are with the lowest energy, whereas among the VIB transition-metal elements, only W atom.[39] This phenomenon predicts that it is more strenuous to maintain the superatomic structures if the systems have too many electrons. Thus, it is reasonable that the lowest energy isomer is not the face-sharing bitetrahexahedral motif, but the C_{2v} symmetry B1 for $W_2@Li_{20}$. Meanwhile, the existence of isosupermolecules gives another way to assemble materials from superatoms, and the binary superatoms are excellent choices as the building blocks, for example, VLi_n (n = 1−13) clusters, the value of n from 8 to 13 corresponding to superatom,[55] promoting the possibility of assembled materials.

Interestingly, when the endohedral transition-metal elements are a hybrid of Ti and W atoms, the face-sharing bitetrahexahedral structure for $TiW@Li_{20}$ is still retained, but with a C_{6v} symmetry because the hetero-Ti and W atoms decrease the symmetry. The corresponding electronic configuration of the $TiW@Li_{20}$ cluster is $(\sigma_{1s})^2(\sigma^*_{1s})^2(\pi_{1p_x,1p_y})^4(\sigma_{1d_{z^2}})^2(\sigma_{1d_{xz,yz}})^4(\delta_{1d_{x^2-y^2,xy}})^4(\pi^*_{1p_x,1p_y})^4(\sigma_{1p_z})^2(\sigma^*_{1p_z})^2(\delta^*_{1d_{x^2-y^2,xy}})^4(\sigma_{2s})^0(\sigma^*_{2s})^0$, similar to the electron filling orders of superatomic molecule $W_2@Li_{20}$ except the orders of $\sigma_{1d_{xz,yz}}$ and $\sigma_{1d_{z^2}}$. The MO diagrams and chemical bonding patterns of $TiW@Li_{20}$ are shown in Figures S3 and S4, respectively, where the energy difference of $\delta^*_{1d_{x^2-y^2,xy}}$ and σ_{2s} forms its HOMO−LUMO gap (0.76 eV/TPSSh), equal to the gap of $Ti_2@Li_{20}$ at the TPSSh/SDD level. Different from them, the hetero-bitetrahexahedral superatomic molecule $TiW@Li_{20}$ produces a dipole moment (1.71 D/TPSSh), as shown in Table 1. The present results can be enhanced by proper selection of the dopants or the building blocks. Consequently, by varying the central transition-metal elements of $M_1M_2@Li_{20}$ (M_1M_2 = Ti and W), their properties can be precisely tuned while with the geometric structures fixed.

4. CONCLUSIONS

A D_{6h} symmetry face-sharing bi-tetrahexahedral motif of superatomic molecules is found via the assembly of two $Ti@Li_{14}$ or $W@Li_{14}$ superatoms along the axis, where the middle six lithium atoms are shared by the two superatoms. Combining CALYSPO structure prediction method and density functional theory calculations, the face-sharing bi-tetrahexahedral $Ti_2@Li_{20}$ and $W_2@Li_{20}$ are proved to be low-energy isomers. According to MO diagrams and chemical bonding patterns, the superatomic molecules $Ti_2@Li_{20}$ or $W_2@Li_{20}$ are formed by quadruple superbonding between two tetrahexahedral superatoms. Interestingly, $Ti_2@Li_{20}$ is identified as a magnetic superatomic molecule with a magnetic moment of 2 μ_B, whereas $W_2@Li_{20}$ remains nonmagnetic. Moreover, when two hetero-tetrahexahedral superatoms $Ti@Li_{14}$ and $W@Li_{14}$ are chosen as the building blocks, the resulting superatomic molecule $TiW@Li_{20}$ still features in a face-sharing bi-tetrahexahedral structure, but with a reduced symmetry of C_{6v} and a net dipole moment (1.71 D/TPSSh). Our findings are encouraging because the superatomic molecules are stable despite plenty of atoms shared between two superatoms as well as no ligand protection. Meanwhile, the properties, such as the HOMO−LUMO gap, magnetic moment, and dipole moment, can be tailored by changing the endohedral transition-metal elements.

■ ASSOCIATED CONTENT

Supporting Information

The Supporting Information is available free of charge on the ACS Publications website at DOI: 10.1021/acs.jpca.9b01855.

Kohn−Sham MO diagrams and AdNDP localized natural bonding orbitals of the three superatomic molecules, namely, two isosupermolecules $Ti_2@Li_{20}$ (D_{2d}, A2) and $W_2@Li_{20}$ (D_{2d}, B4), and one hetero-superatomic molecule $TiW@Li_{20}$ (PDF)

■ AUTHOR INFORMATION

Corresponding Author

*E-mail: ylj_gdou@126.com.

ORCID

Lijuan Yan: 0000-0002-0950-2547

Notes

The author declares no competing financial interest.

■ ACKNOWLEDGMENTS

This work is supported by the Special Foundation for Theoretical Physics Research Program of China (no. 11847119) and the Innovation and Strong School Research Project of Guangdong Ocean University (no. GDOU2017052621).

■ REFERENCES

(1) Khanna, S. N.; Jena, P. Atomic Clusters: Building Blocks for a Class of Solids. *Phys. Rev. B: Condens. Matter Mater. Phys.* **1995**, *51*, 13705−13716.

(2) Claridge, S. A.; Castleman, A. W.; Khanna, S. N.; Murray, C. B.; Sen, A.; Weiss, P. S. Cluster-Assembled Materials. *ACS Nano* **2009**, *3*, 244−255.

(3) Castleman, A. W.; Khanna, S. N. Clusters, Superatoms, and Building Blocks of New Materials. *J. Phys. Chem. C* **2009**, *113*, 2664−2675.

(4) Bergeron, D. E.; Castleman, A. W., Jr.; Morisato, T.; Khanna, S. N. Formation of $Al_{13}I^-$: Evidence for the Superhalogen Character of Al_{13}. *Science* **2004**, *304*, 84−87.

(5) Ekardt, W. Work Function of Small Metal Particles: Self-Consistent Spherical Jellium-Background Model. *Phys. Rev. B: Condens. Matter Mater. Phys.* **1984**, *29*, 1558−1564.

(6) Ekardt, W. Theory of Electronic Excitations in Coated Metal Particles: Jellium-on-Jellium Model. *Phys. Rev. B: Condens. Matter Mater. Phys.* **1986**, *34*, 526−533.

(7) Knight, W. D.; Clemenger, K.; de Heer, W. A.; Saunders, W. A.; Chou, M. Y.; Cohen, M. L. Electronic Shell Structure and Abundances of Sodium Clusters. *Phys. Rev. Lett.* **1984**, *52*, 2141−2143.

(8) Leuchtner, R. E.; Harms, A. C.; Castleman, A. W. Thermal Metal Cluster Anion Reactions: Behavior of Aluminum Clusters with Oxygen. *J. Chem. Phys.* **1989**, *91*, 2753−2754.

(9) Jin, R. Quantum Sized, Thiolate-Protected Gold Nanoclusters. *Nanoscale* **2010**, *2*, 343−362.

(10) Maity, P.; Xie, S.; Yamauchi, M.; Tsukuda, T. Stabilized Gold Clusters: From Isolation toward Controlled Synthesis. *Nanoscale* **2012**, *4*, 4027−4037.

(11) Heaven, M. W.; Dass, A.; White, P. S.; Holt, K. M.; Murray, R. W. Crystal Structure of the Gold Nanoparticle $[N(C_8H_{17})_4][Au_{25}(SCH_2CH_2Ph)_{18}]$. *J. Am. Chem. Soc.* **2008**, *130*, 3754−3755.

(12) Zhu, M.; Aikens, C. M.; Hollander, F. J.; Schatz, G. C.; Jin, R. Correlating the Crystal Structure of a Thiol-Protected Au_{25} Cluster and Optical Properties. *J. Am. Chem. Soc.* **2008**, *130*, 5883−5885.

(13) Shichibu, Y.; Konishi, K. HCl-Induced Nuclearity Convergence in Diphosphine-Protected Ultrasmall Gold Clusters: A Novel

DOI: 10.1021/acs.jpca.9b01855
J. Phys. Chem. A 2019, 123, 5517−5524

Synthetic Route to "Magic-Number" Au_{13} Clusters. *Small* **2010**, *6*, 1216−1220.
(14) Nobusada, K.; Iwasa, T. Oligomeric Gold Clusters with Vertex-Sharing Bi- and Triicosahedral Structures. *J. Phys. Chem. C* **2007**, *111*, 14279−14282.
(15) Shichibu, Y.; Negishi, Y.; Watanabe, T.; Chaki, N. K.; Kawaguchi, H.; Tsukuda, T. Biicosahedral Gold Clusters $[Au_{25}(PPh_3)_{10}(SC_nH_{2n+1})_5Cl_2]^{2+}$ (n=2-18): A Stepping Stone to Cluster-Assembled Materials. *J. Phys. Chem. C* **2007**, *111*, 7845−7847.
(16) Lopez-Acevedo, O.; Tsunoyama, H.; Tsukuda, T.; Häkkinen, H.; Aikens, C. M. Chirality and Electronic Structure of the Thiolate-Protected Au_{38} Nanocluster. *J. Am. Chem. Soc.* **2010**, *132*, 8210−8218.
(17) Qian, H.; Eckenhoff, W. T.; Zhu, Y.; Pintauer, T.; Jin, R. Total Structure Determination of Thiolate-Protected Au_{38} Nanoparticles. *J. Am. Chem. Soc.* **2010**, *132*, 8280−8281.
(18) Qian, H.; Zhu, Y.; Jin, R. Isolation of Ubiquitous $Au_{40}(SR)_{24}$ Clusters from the 8 kDa Gold Clusters. *J. Am. Chem. Soc.* **2010**, *132*, 4583−4585.
(19) Malola, S.; Lehtovaara, L.; Knoppe, S.; Hu, K.-J.; Palmer, R. E.; Bürgi, T.; Häkkinen, H. $Au_{40}(SR)_{24}$ Cluster as a Chiral Dimer of 8-Electron Superatoms: Structure and Optical Properties. *J. Am. Chem. Soc.* **2012**, *134*, 19560−19563.
(20) Koyasu, K.; Akutsu, M.; Mitsui, M.; Nakajima, A. Selective Formation of MSi_{16} (M=Sc, Ti, and V). *J. Am. Chem. Soc.* **2005**, *127*, 4998−4999.
(21) Torres, M. B.; Fernández, E. M.; Balbás, L. C. Theoretical Study of Isoelectronic Si_nM clusters (M=Sc−,Ti,V+;n=14−18). *Phys. Rev. B: Condens. Matter Mater. Phys.* **2007**, *75*, 205425.
(22) Shibuta, M.; Ohta, T.; Nakaya, M.; Tsunoyama, H.; Eguchi, T.; Nakajima, A. Chemical Characterization of an Alkali-Like Superatom Consisting of a Ta-Encapsulating Si_{16} Cage. *J. Am. Chem. Soc.* **2015**, *137*, 14015−14018.
(23) Sen, A.; Sen, P. Properties of Highly Oriented Pyrolytic Graphite Supported $TaSi_{16}$ Clusters: A Density Functional Investigation. *J. Phys. Chem. C* **2017**, *121*, 28490−28497.
(24) Tsunoyama, H.; Akatsuka, H.; Shibuta, M.; Iwasa, T.; Mizuhata, Y.; Tokitoh, N.; Nakajima, A. Development of Integrated Dry−Wet Synthesis Method for Metal Encapsulating Silicon Cage Superatoms of $M@Si_{16}$ (M = Ti and Ta). *J. Phys. Chem. C* **2017**, *121*, 20507−20516.
(25) Tsunoyama, H.; Shibuta, M.; Nakaya, M.; Eguchi, T.; Nakajima, A. Synthesis and Characterization of Metal-Encapsulating Si_{16} Cage Superatoms. *Acc. Chem. Res.* **2018**, *51*, 1735−1745.
(26) Gong, X. G.; Kumar, V. Enhanced Stability of Magic Clusters: A Case Study of Icosahedral $Al_{12}X$, X=B, Al, Ga, C, Si, Ge, Ti, As. *Phys. Rev. Lett.* **1993**, *70*, 2078−2081.
(27) Akutsu, M.; Koyasu, K.; Atobe, J.; Hosoya, N.; Miyajima, K.; Mitsui, M.; Nakajima, A. Experimental and Theoretical Characterization of Aluminum-Based Binary Superatoms of $Al_{12}X$ and Their Cluster Salts. *J. Phys. Chem. A* **2006**, *110*, 12073−12076.
(28) Molina, B.; Soto, J. R.; Castro, J. J. Stability and Nonadiabatic Effects of the Endohedral Clusters $X@Al_{12}$ (X = B, C, N, Al, Si, P) with 39, 40, and 41 Valence Electrons. *J. Phys. Chem. C* **2012**, *116*, 9290−9299.
(29) Reveles, J. U.; Baruah, T.; Zope, R. R. $Al_{12}Cu$ Superatom as Stable Building Block of Ionic Salts. *J. Phys. Chem. C* **2015**, *119*, 5129−5137.
(30) Sun, W.-M.; Wu, D.; Li, X.-H.; Li, Y.; Chen, J.-H.; Li, C.-Y.; Liu, J.-Y.; Li, Z.-R. Quasi-Chalcogen Characteristics of $Al_{12}Be$: A New Member of the Three-Dimensional Periodic Table. *J. Phys. Chem. C* **2016**, *120*, 2464−2471.
(31) Akutsu, M.; Koyasu, K.; Atobe, J.; Miyajima, K.; Mitsui, M.; Tsunoyama, H.; Nakajima, A. Geometric and Electronic Properties of Si-Atom Doped Al Clusters: Robustness of Binary Superatoms against Charging. *Phys. Chem. Chem. Phys.* **2017**, *19*, 20401−20411.
(32) Ghosh, A.; Mohammed, O. F.; Bakr, O. M. Atomic-Level Doping of Metal Clusters. *Acc. Chem. Res.* **2018**, *51*, 3094−3103.
(33) Cheng, L.; Yang, J. Communication: New Insight into Electronic Shells of Metal Clusters: Analogues of Simple Molecules. *J. Chem. Phys.* **2013**, *138*, 141101.
(34) Cheng, L.; Ren, C.; Zhang, X.; Yang, J. New Insight into the Electronic Shell of $Au_{38}(SR)_{24}$: A Superatomic Molecule. *Nanoscale* **2013**, *5*, 1475−1478.
(35) Yuan, Y.; Cheng, L.; Yang, J. Electronic Stability of Phosphine-Protected Au_{20} Nanocluster: Superatomic Bonding. *J. Phys. Chem. C* **2013**, *117*, 13276−13282.
(36) Cheng, L.; Zhang, X.; Jin, B.; Yang, J. Superatom-Atom Super-Bonding in Metallic Clusters: A New Look to the Mystery of an Au_{20} Pyramid. *Nanoscale* **2014**, *6*, 12440−12444.
(37) Yan, L.; Cheng, L.; Yang, J. Tetrahedral Au_{17}^+: A Superatomic Molecule with a Au_{13} Fcc Core. *J. Phys. Chem. C* **2015**, *119*, 23274−23278.
(38) Wang, H.; Cheng, L. Quintuple Super Bonding between the Superatoms of Metallic Clusters. *Nanoscale* **2017**, *9*, 13209−13213.
(39) Yan, L.; Liu, J.; Shao, J. Superatomic Properties of Transition-Metal-Doped Tetrahexahedral Lithium Clusters: $TM@Li_{14}$. *Mol. Phys.* **2019**, DOI: 10.1080/00268976.2019.1592256.
(40) Lv, J.; Wang, Y.; Zhu, L.; Ma, Y. Particle-Swarm Structure Prediction on Clusters. *J. Chem. Phys.* **2012**, *137*, 084104.
(41) Frisch, M. J.; Trucks, G. W.; Schlegel, H. B.; Scuseria, G. E.; Robb, M. A.; Cheeseman, J. R.; Scalmani, G.; Barone, V.; Mennucci, B.; Petersson, G. A. e. a. *Gaussian 16*, Revision B.01; Gaussian, Inc.: Wallingford, Ct, 2016.
(42) Weymuth, T.; Couzijn, E. P. A.; Chen, P.; Reiher, M. New Benchmark Set of Transition-Metal Coordination Reactions for the Assessment of Density Functionals. *J. Chem. Theory Comput.* **2014**, *10*, 3092−3103.
(43) Dohm, S.; Hansen, A.; Steinmetz, M.; Grimme, S.; Checinski, M. P. Comprehensive Thermochemical Benchmark Set of Realistic Closed-Shell Metal Organic Reactions. *J. Chem. Theory Comput.* **2018**, *14*, 2596−2608.
(44) Perdew, J. P.; Wang, Y. Accurate and Simple Analytic Representation of the Electron-Gas Correlation Energy. *Phys. Rev. B: Condens. Matter Mater. Phys.* **1992**, *45*, 13244−13249.
(45) Zhao, Y.; Truhlar, D. G. A New Local Density Functional for Maingroup Thermochemistry, Transition Metal Bonding, Thermochemical Kinetics, and Noncovalent Interactions. *J. Chem. Phys.* **2006**, *125*, 194101.
(46) Staroverov, V. N.; Scuseria, G. E.; Tao, J.; Perdew, J. P. Comparative Assessment of a New Nonempirical Density Functional: Molecules and Hydrogen-Bonded Complexes. *J. Chem. Phys.* **2003**, *119*, 12129−12137.
(47) Hay, P. J.; Wadt, W. R. Ab Initio Effective Core Potentials for Molecular Calculations. Potentials for the Transition Metal Atoms Sc to Hg. *J. Chem. Phys.* **1985**, *82*, 270−283.
(48) Lu, T.; Chen, F. Multiwfn: A Multifunctional Wavefunction Analyzer. *J. Comput. Chem.* **2012**, *33*, 580−592.
(49) Liu, L.; Li, P.; Yuan, L.-F.; Cheng, L.; Yang, J. From Isosuperatoms to Isosupermolecules: New Concepts in Cluster Science. *Nanoscale* **2016**, *8*, 12787−12792.
(50) Reveles, J. U.; Clayborne, P. A.; Reber, A. C.; Khanna, S. N.; Pradhan, K.; Sen, P.; Pederson, M. R. Designer Magnetic Superatoms. *Nat. Chem.* **2009**, *1*, 310−315.
(51) Zhang, X.; Wang, Y.; Wang, H.; Lim, A.; Gantefoer, G.; Bowen, K. H.; Reveles, J. U.; Khanna, S. N. On the Existence of Designer Magnetic Superatoms. *J. Am. Chem. Soc.* **2013**, *135*, 4856−4861.
(52) Huang, X.; Zhao, J.; Su, Y.; Chen, Z.; King, R. B. Design of Three-Shell Icosahedral Matryoshka Clusters $A@B_{12}@A_{20}$ (A=Sn, Pb; B=Mg, Zn, Cd, Mn). *Sci. Rep.* **2015**, *4*, 6915.
(53) Pradhan, K.; Reveles, J. U.; Sen, P.; Khanna, S. N. Enhanced Magnetic Moments of Alkali Metal Coated Sc Clusters: New Magnetic Superatoms. *J. Chem. Phys.* **2010**, *132*, 124302.
(54) Zubarev, D. Y.; Boldyrev, A. I. Developing Paradigms of Chemical Bonding: Adaptive Natural Density Partitioning. *Phys. Chem. Chem. Phys.* **2008**, *10*, 5207−5217.

DOI: 10.1021/acs.jpca.9b01855
J. Phys. Chem. A 2019, 123, 5517−5524

(55) Zhang, M.; Zhang, J.; Feng, X.; Zhang, H.; Zhao, L.; Luo, Y.; Cao, W. Magnetic Superatoms in VLi_n (n = 1-13) Clusters: A First-Principles Prediction. *J. Phys. Chem. A* **2013**, *117*, 13025−13036.
(56) Fournier, R.; Bo Yi Cheng, J.; Wong, A. Theoretical Study of the Structure of Lithium Clusters. *J. Chem. Phys.* **2003**, *119*, 9444−9454.

DOI: 10.1021/acs.jpca.9b01855
J. Phys. Chem. A 2019, 123, 5517−5524